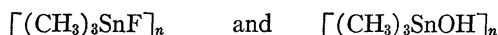


The x-ray diffraction crystal structures^{18,19} of



show that these compounds are one-dimensional linear-polymeric chains held together by weak van der Waals forces between methyl groups in neighboring chains, whereas $(\text{C}_6\text{H}_5)_3\text{SnCl}$ is a weakly bonded three-dimensional monomeric unit. The structure of $[(\text{CH}_3)_3\text{SnF}]_n$ is shown in Fig. 2, where a set of lattice-dynamic principal axes are indicated. In an intermediate temperature range T_2 such linear polymers have $\langle u_r^2 \rangle_x \approx \langle u_r^2 \rangle_y > \langle u_r^2 \rangle_z$, the eccentricity of the vibrational ellipsoid being maximized.^{20,21} At low and high temperatures T_1 and T_3 $\langle u_r^2 \rangle_x \approx \langle u_r^2 \rangle_y \approx \langle u_r^2 \rangle_z$, the thermal motion being nearly a vibrational sphere. For a monomeric material, $\langle u_r^2 \rangle_x \approx \langle u_r^2 \rangle_y \approx \langle u_r^2 \rangle_z$ at almost

¹⁸ H. C. Clark, R. J. O'Brien, and J. Trotter, Proc. Chem. Soc. 1964, 85 (1964); J. Chem. Soc. 1964, 2332 (1964).

¹⁹ N. Kasai, K. Yasuda, and R. Okawara, J. Organometal. Chem. (Amsterdam) 3, 172 (1965).

²⁰ E. Sandor, Acta Cryst. 15, 463 (1962).

²¹ K. Lonsdale, Acta Cryst. 14, 37 (1961).

all temperatures. From Fig. 1, it is seen that the linear-chain compounds display a strong temperature-dependent Karyagin effect due to the significant anisotropic thermal behavior of the linear polymers in T_2 . For $[(\text{CH}_3)_3\text{SnF}]_n$, $d(I_2/I_1)/dT < 0$, whereas

$$d(I_2/I_1)/dT > 0$$

for $[(\text{CH}_3)_3\text{SnOH}]_n$ in the range T_2 . If λ_{\pm} is constant in T_2 and $\eta \neq 1$, then a difference in the sign of $d(I_2/I_1)/dR$ indicates that $\delta E_{z'}/\delta z'$ in $(\text{CH}_3)_3\text{SnOH}$ and $(\text{CH}_3)_3\text{SnF}$ probably have opposite signs, and hence the $(\pm \frac{3}{2}, \frac{1}{2} +)$ and the $(\pm \frac{1}{2}, \frac{3}{2} +)$ levels are energetically reversed in these two compounds. At low temperatures, i.e., in the range R_1 , $(I_2/I_1) \approx 1$ and $d(I_2/I_1)/dR \rightarrow 0$, and the Karyagin effect vanishes in these chain compounds. That $(I_2/I_1) \approx 1$ and $d(I_2/I_1)/dR \approx 0$ for $(\text{C}_6\text{H}_5)_3\text{SnCl}$ reflects the almost isotropic thermal behavior of the Sn^{119} atom in this compound and a negligible Karyagin effect is observed. This result is in agreement with the evidence found in Ref. 8 but substantially disagrees with that of Goldanskii *et al.*

Stopping Cross Section in Carbon of 0.2–1.5-MeV Atoms with $21 \leq Z_1 \leq 39$

P. HVELPLUND AND B. FASTRUP

Institute of Physics, University of Aarhus, Aarhus C, Denmark

(Received 29 August 1967)

The stopping cross section $S = dE/NdR$ in thin carbon foils has been measured for ions with $21 \leq Z_1 \leq 39$ and with energies from 200 to 1500 keV. The experimental data have been corrected numerically for nuclear stopping, and the electronic stopping obtained is compared with theory. At constant projectile velocity, the periodic dependence of the electronic stopping cross section on the atomic number Z_1 of the incoming ions, previously reported for $Z_1 \leq 20$, is seen also in the present extended Z_1 range. The data show that the amplitude of the successive oscillations is approximately constant over the whole Z_1 range. The relative amplitude, however, tends to decrease with increasing velocity. The relative accuracy of the results is about 3%.

INTRODUCTION

THE slowing-down of energetic atomic particles in matter is determined by two processes: electronic encounters and nuclear encounters. In the high-energy region, electronic stopping predominates, and the Bethe–Bloch formula describes the stopping cross section. However, in the low-energy region, i.e., for velocities below $v_0 Z_1^{2/3}$, where v_0 is the Bohr velocity, the electronic stopping cross section is proportional to the velocity of the incoming ion, and the nuclear stopping cross section becomes increasingly important when the velocity is reduced. For example, the energy at which the nuclear stopping becomes equal to the electronic stopping in carbon is 220 keV for Sc and 580 keV for Kr.

The theory of electronic stopping at low velocities has been given by Fermi and Teller¹ and by Lindhard² for an electron gas, and by Lindhard and Scharff³ and by Firsov⁴ for the atomic case.

The treatment by Lindhard and Scharff is based on the Thomas–Fermi statistical model for the atom, and they quote the following result for the electronic stopping cross section valid for ion velocities less than $v_0 Z_1^{2/3}$:

$$S_e = \xi_e 8\pi e^2 a_0 (Z_1 Z_2 / Z) (v/v_0) \quad (Z^{2/3} = Z_1^{2/3} + Z_2^{2/3}),$$

¹ E. Fermi and E. Teller, Phys. Rev. 72, 399 (1947).

² J. Lindhard, Kgl. Danske Videnskab Selskab, Mat.-Fys. Medd. 28, 8 (1954).

³ J. Lindhard and M. Scharff, Phys. Rev. 124, 128 (1961).

⁴ O. B. Firsov, Zh. Eksperim. i Teor. Fiz. 36, 1517 (1959) [English transl.: Soviet Phys.—JETP 9, 1076 (1959)].

where a_0 is the Bohr radius, Z_2 the atomic number of the target atoms, e the electron charge, and ξ_e a constant of order 1–2, which may vary approximately as $Z_1^{1/6}$.

From a semiclassical Thomas–Fermi treatment, Firsov calculated the electronic stopping cross section for a specified impact parameter. By performing an integration over all impact parameters, the result obtained is

$$S_e = 5.15 \times 10^{-15} (Z_1 + Z_2) (v/v_0) \text{ eV cm}^2/\text{atom},$$

valid when the atomic numbers of the colliding particles differ by no more than a factor of 4.

The two theoretical expressions show the stopping cross section to be a monotonic function of Z_1 since both are based on statistical models of the atom.

In 1962, Teplova *et al.*⁵ found experimentally that the ranges of different light projectiles in atmospheric air showed a nonmonotonic dependence on Z_1 . Shortly after, Ormrod and Duckworth⁶ subjected the Lindhard–Scharff theory to a systematic experimental investigation by determining the electronic stopping cross sections in carbon for $Z_1 \leq 12$ and $10 \text{ keV} \leq E \leq 140 \text{ keV}$. The results revealed an oscillatory dependence of S_e on Z_1 for constant projectile velocity with an amplitude of about 40%. However, the average values were in good agreement with the theoretical predictions. Ormrod *et al.*⁷ and Macdonald *et al.*⁸ have shown that for boron, carbon, and aluminum targets, the periodic structure is almost insensitive to the choice of Z_2 . Unpublished data by Ormrod, Macdonald, and Duckworth⁹ have confirmed this finding also for nickel targets.

Stopping-power measurements by Fastrup *et al.*¹⁰ (in the following referred to as I) in carbon with $Z_1 \leq 20$ at energies up to 1 MeV have shown that the relative amplitudes of the oscillations decrease with increasing velocity of the ions. It was suggested that at higher relative velocities, atomic shells begin to overlap, causing the shell effect to be less pronounced.

Range studies in an oriented tungsten crystal by Eriksson *et al.*¹¹ for $Z_1 = 11, 15, 19, 24, 29, 35, 36, 37, 51, 54,$ and 55 showed oscillations in the electronic stopping cross section for channeled ions similar to those seen in amorphous carbon. The steering mechanism of the atomic strings prevents the aligned ions

from close collisions with the target atoms with the result that the observed electronic stopping is reduced by a factor of about 3 compared with the random case.

Since the statistical description of the atoms on which the calculations are based should improve with increasing atomic number of the incoming ions, it would be expected that the amplitudes of the oscillations might be reduced for higher Z_1 . To check this hypothesis, an experimental study of S_e , including ions with Z_1 up to 39, was carried out in amorphous carbon. Measurements were made at ion energies ranging from 200 to 1500 keV. In the experimental setup, only a small fraction of the transmitted beam was admitted to the analyzing magnet. As will be shown later, it was possible by a careful study of the energy-loss distributions to correct the observed data for nuclear stopping and thus the electronic stopping was obtained.

APPARATUS

The ions were produced in a universal ion source and accelerated in the Aarhus 600-keV heavy-ion accelerator. Those with the desired momentum were selected in a 75° double-focusing sector magnet with a radius of 150 cm. After acceleration and deflection of the ions, the direction was determined to within $\frac{1}{3}^\circ$ by two moveable apertures a and b (Fig. 1). By selecting up to triply charged ions, it was possible to extend the energy range up to 1500 keV.

The target foils of amorphous carbon were fabricated at the Hebrew University of Jerusalem. The thickness of the foils ranged from approximately 5 to $10 \mu\text{g}/\text{cm}^2$. The foils were mounted on a frame with 8 holes which was inserted in a moveable foil holder. This arrangement made it possible to irradiate up to 8 self-supporting areas of the foil without disturbing the vacuum in the target chamber. The foils were positioned in the beam path at the focal point of the bending magnet. A liquid-air cooling trap was immersed in the target chamber to prevent buildup of surface layers on the foils during irradiation. The working pressure in the target chamber was better than 10^{-5} Torr.

The energy of the ions emerging from the foil was determined in a 60-cm-radius, 90° double-focusing magnet. At the focal point of this magnet, a Faraday cage with a 5-mm slit was placed with the slit perpendicular to the plane of the beam through the magnet. This gave a resolution of approx. 0.5%. The magnetic field was determined by a Hall probe with linearity better than 0.2%.

EXPERIMENTAL METHOD AND DATA TREATMENT

The energy loss of the ions penetrating the foil was determined in the following way: By means of an X–Y curve plotter, the current to the Faraday cage, with and without the foil positioned in the beam, was

⁵ Ya. A. Teplova, V. S. Nikolaev, I. S. Dmitriv, and N. L. Fateeva, *Zh. Eksperim. i Teor. Fiz.* **42**, 44 (1962) [English transl.: *Soviet Phys.—JETP* **15**, 31 (1962)].

⁶ J. H. Ormrod and H. E. Duckworth, *Can. J. Phys.* **41**, 1424 (1963).

⁷ J. H. Ormrod, J. R. Macdonald, and H. E. Duckworth, *Can. J. Phys.* **43**, 275 (1965).

⁸ J. R. Macdonald, J. H. Ormrod, and H. E. Duckworth, *Z. Naturforsch.* **21a**, 130 (1966).

⁹ J. R. Macdonald (private communication).

¹⁰ B. Fastrup, P. Hvelplund, and C. A. Sautter, *Kgl. Danske Videnskab Selskab, Mat.-Fys. Medd.* **35**, 10 (1966).

¹¹ L. Eriksson, J. A. Davies, and P. Jespersgaard, *Phys. Rev.* **161**, 219 (1967).

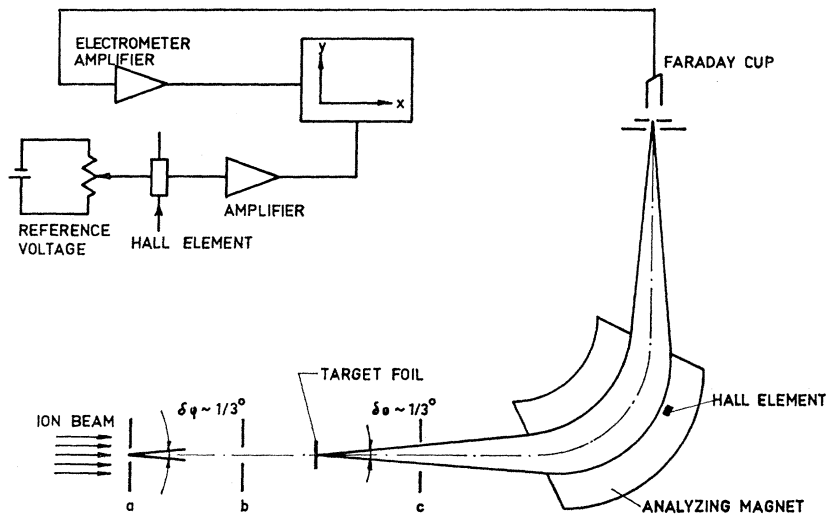


FIG. 1. General diagram of apparatus. a, b, and c indicate the limiting apertures in the setup.

plotted as a function of the magnetic field in the analyzing magnet. The resulting momentum distribution was converted to an energy distribution, which is shown in Fig. 2.

From the energy curves with and without the foil placed in the beam, the most probable energy loss ΔE_0 is determined.

The stopping cross section S_0 is then defined as

$$S_0 = (1/N) (\Delta E_0 / \Delta R) \quad \text{at the energy } E = E_i - \Delta E_0 / 2,$$

where E_i is the energy of the ions incident on the foil, N the number of target atoms per unit volume, and ΔR the thickness of the foil. The difference between $\Delta E_0 / \Delta R$ and $-dE/dR$ was, in all cases reported here, less than 0.1% and thus neglected.

The energy profile of the ions emerging from the foil may be separated into two parts: a Gaussian distribution and a low-energy tail distribution. By taking the mirror image of the high-energy side of the experimental curve with respect to a line through the most probable value, a good approximation to a Gaussian curve was

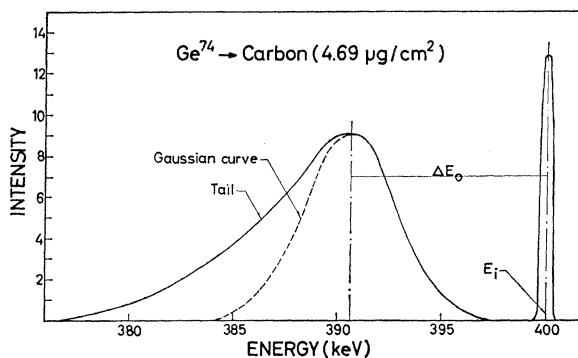


FIG. 2. Energy profiles of the incident and transmitted Ge^{74} ions.

obtained (Fig. 2). According to Bohr¹² and Williams,¹³ the Gaussian distribution results from a combination of electronic collisions and soft nuclear collisions while the tail distribution arises from violent nuclear collisions.

The mean energy loss related to the Gaussian-distributed encounters corresponds to a good approximation to the most probable value of the observed energy loss ΔE_0 , i.e.,

$$\Delta E_0 \approx \Delta E_e + \Delta E_n^*,$$

where ΔE_e is the mean electronic energy loss and ΔE_n^* the mean energy loss of the Gaussian nuclear collision:

$$\Delta E_n^* = N \Delta R \int_0^{T^*} T d\sigma. \quad (1)$$

Here, $d\sigma$ is the differential cross section for an energy transfer T during a collision and T^* is an effective upper limit for energy transfers contributing to the Gaussian energy-loss distribution. Bohr¹² estimated T^* to be approximately equal to the nuclear Gaussian energy straggling Ω_n^* , i.e.,

$$(T^*)^2 \approx (\Omega_n^*)^2 \approx N \Delta R \int_0^{T^*} T^2 d\sigma, \quad (2)$$

provided $\Delta E_0 \ll E_i$. If Eqs. (1) and (2) are combined with the application of a Thomas-Fermi scattering cross section,¹⁴ the following result is obtained:

$$S_n^* = \int_0^{T^*} T d\sigma = 2.57 \times 10^{-16} \frac{A_1 Z_1^2 Z_2^2 \epsilon^*}{A_2 E_i} I(\epsilon^*) \quad \text{eV cm}^2/\text{atom}. \quad (3)$$

¹² N. Bohr, *Phil. Mag.* **25**, 10 (1913); N. Bohr, *Kgl. Danske Videnskab Selskab, Mat.-Fys. Medd.* **18**, 8 (1948).

¹³ E. J. Williams, *Proc. Roy. Soc. (London)* **A125**, 420 (1929).

¹⁴ J. Lindhard, M. Scharff, and H. E. Schiött, *Kgl. Danske Videnskab Selskab, Mat.-Fys. Medd.* **33**, 14 (1963).

TABLE I. Stopping cross sections in amorphous carbon for the atoms indicated at various energies. The foil thickness is Δx . S_n^* is the computed nuclear stopping correction, and S_e is the derived electronic stopping.

Atom	E (keV)	Δx ($\mu\text{g}/\text{cm}^2$)	S_n^* (10^{-14} eV $\text{cm}^2/\text{at.}$)	S_e (10^{-14} eV $\text{cm}^2/\text{at.}$)	Atom	E (keV)	Δx ($\mu\text{g}/\text{cm}^2$)	S_n^* (10^{-14} eV $\text{cm}^2/\text{at.}$)	S_e (10^{-14} eV $\text{cm}^2/\text{at.}$)
Sc ⁴⁵	230	9.85	1.08	7.26	Co ⁵⁹	242	6.03	1.22	3.57
	377	9.70	0.66	8.81		393	4.50	0.64	4.62
	574	9.80	0.46	10.00		590	6.94	0.62	6.04
	771	9.85	0.36	11.63		790	5.71	0.38	6.97
	875	8.28	0.26	11.88		1185	5.53	0.24	9.68
	1170	9.18	0.22	13.34					
Ti ⁴⁷	240	6.72	0.86	6.35	Cu ⁶⁵	396	3.82	0.60	3.97
	388	6.62	0.54	7.60		594	4.62	0.50	5.81
	575	9.18	0.48	9.62		792	4.51	0.36	7.07
	775	8.28	0.32	10.69		1189	4.51	0.24	10.04
	973	8.28	0.26	11.74		1485	5.18	0.22	10.95
Cr ⁵²	390	5.25	0.54	6.63	Ge ⁷⁴	395	4.69	1.00	3.41
	590	4.76	0.32	8.34		495	5.00	0.88	3.59
	789	4.56	0.22	9.60		890	5.74	0.58	6.75
	1185	5.00	0.16	11.83		1185	6.71	0.50	8.60
	1485	5.25	0.14	13.05		1486	5.55	0.32	9.33
Mn ⁵⁵	384	9.05	0.98	5.72	Br ⁷⁹	590	5.45	0.96	6.74
	585	7.52	0.56	7.47		886	5.69	0.68	8.63
	880	8.85	0.42	9.08		1185	5.81	0.52	9.97
	1174	9.05	0.32	10.94		1482	5.81	0.40	11.85
Fe ⁵⁶	238	8.26	1.64	4.05	Kr ⁸⁶	590	5.32	1.04	6.50
	387	9.14	1.10	5.02		888	5.10	0.66	8.48
	878	8.82	0.48	8.76		1185	5.18	0.50	10.36
	1175	9.30	0.36	10.13		1485	5.32	0.42	10.87
	1470	9.30	0.28	11.52					
				Y ⁸⁹	488	4.69	1.26	8.02	
					785	5.55	0.98	9.80	
					1180	6.71	0.82	12.02	
					1477	6.14	0.58	12.89	

(For more detailed treatment and analysis, refer to I). Here, A_1 and A_2 are the atomic mass numbers of the projectile and the target atoms, respectively, E_i is the incident beam energy in keV, $I(\epsilon) = d\epsilon/d\rho$ is the nuclear stopping cross section in reduced units,¹⁴ and

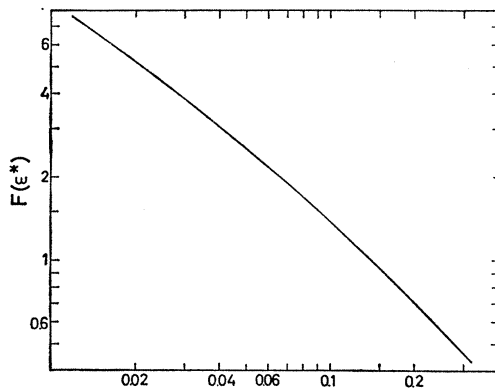


FIG. 3.

$$F(\epsilon^*) = \int_0^{\epsilon^*} f(t^{1/2}) dt^{1/2} / (\epsilon^*)^4,$$

where $f(t^{1/2})$ has been displayed graphically by Lindhard *et al.* in Ref. 14.

$\epsilon^* = \epsilon(T^*/T_{\max})^{1/2}$ is derived from $F(\epsilon^*) = 1/N\Delta R\pi a^2$, obtained from Eq. (2). $T_{\max} = 4M_1M_2E/(M_1+M_2)^2$ is the maximum energy transfer and $a = a_0 \times 0.8853 \times (Z_1^{2/3} + Z_2^{2/3})^{-1/2}$ is the screening distance of the ion-atom potential. The function $F(\epsilon^*)$ is displayed in Fig. 3.

The small acceptance angle of the analyzing magnet ($\frac{1}{3}^\circ$) excludes from analysis most of the particles which have experienced violent collisions. However, as is shown in the detailed analysis in I, the Gaussian part of the total energy loss of the distribution of the emerging ions is not affected by the small acceptance angle, whereas the tail distribution may be radically distorted.

The extension of the earlier data ($Z_1 \leq 20$) in I to higher Z_1 values ($Z_1 \leq 39$) at the same projectile velocities was made possible by incorporating acceleration of up to triply charged ions. The contribution from nuclear stopping was kept low by using thin carbon foils (from 5 to 10 $\mu\text{g}/\text{cm}^2$). The thickness of the foil was calculated from the energy loss of 400-keV Ar ions. At 400 keV, the nuclear stopping is small compared with the electronic stopping for the Ar ions in the thin carbon foils. The stopping cross section for 400-keV Ar ions in carbon was taken from I to be 8.5×10^{-14} eV $\text{cm}^2/\text{atom} \pm 4\%$. This value, in turn,

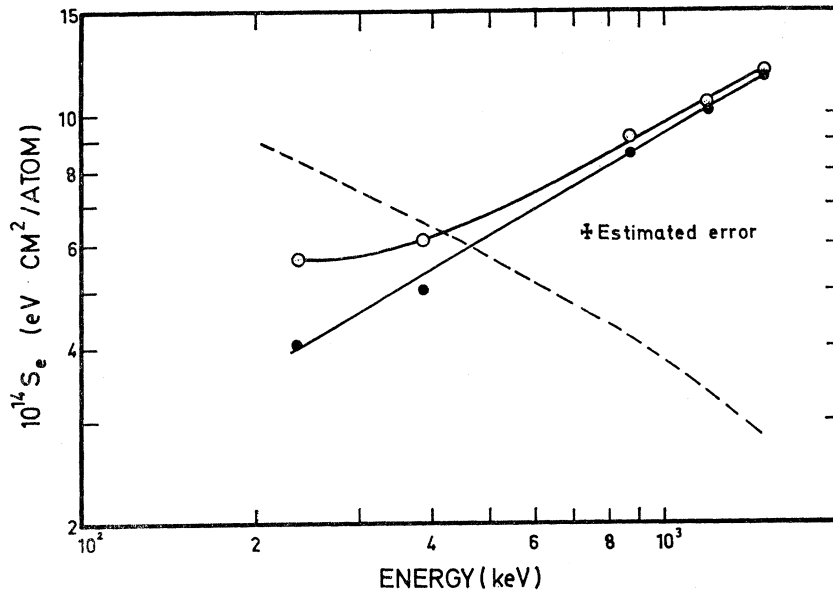


FIG. 4. Stopping cross section for Fe^{56} in carbon. \circ , measured stopping cross section S_0 . \bullet , electronic stopping cross section $S_e = S_0 - S_n^*$, where S_n^* is the computed nuclear stopping correction [Eq. (3)]. Dashed curve indicates theoretical total nuclear stopping cross section

$$S_n = \int_0^{T_{\max}} T d\sigma$$

[Lindhard and Scharff (Ref. 3)].

corresponded to a stopping cross section of 1.26×10^{-14} eV cm²/atom in carbon for 150-keV protons. The relative error in the thickness of the measured foil was estimated to be less than 3%, and the absolute error less than 5%. The change in thickness during irradiation was examined by measuring the energy loss of 400-keV Ar ions before and after irradiation and in no cases was the change greater than 1%.

RESULTS AND DISCUSSION

The stopping cross sections are listed in Table I, together with the measured foil thicknesses and the applied nuclear correction. The relative accuracy of the observed stopping cross section S_0 was established within 3% and, in most cases, this also applies to the evaluated stopping cross section S_e , the only exception being the cases where the nuclear correction is not small compared with S_e , i.e., for large Z_1 values and small projectile energies. As an example, Fig. 4 shows the observed S_0 data for Fe^{56} against energy together with the corrected data for electronic stopping. It is noted that even in the case of considerable nuclear correction, the S_e values in a log-log plot fall on a straight line determined by the S_e data taken at high energies, where the nuclear correction is small. This supports the dependability of the applied correction. For comparison, the total nuclear stopping cross section S_n is also shown in Fig. 4 and it is seen that the applied nuclear correction S_n^* is only a small fraction of S_n . The relative accuracy of the electronic stopping cross section for the reported data is estimated to be better than 4% and the absolute accuracy is better than 7%.

The observed electronic stopping cross sections have been fitted to an equation of the form $S_e = kE^p$ where,

according to the theories by Lindhard and Scharff³ and by Firsov,⁴ p is 0.5. The derived experimental p value for each projectile is plotted in Fig. 5 together with the earlier results for $Z_1 \leq 20$ from I. It is noted that there are some correlation between p values for adjacent elements, indicating that $p(Z_1)$ has an oscillatory structure. The maximum deviation from the theoretical value of 0.5 is 0.35 at $Z_1 = 32$. As is stated in I, it is probable that p depends slightly on the energy with an average not far from 0.5 in an extended energy range covering several decades.

According to the theories based on the Thomas-Fermi statistical model, S_e varies smoothly and monotonically with Z_1 at constant common velocity. In Fig. 6, our experimental S_e data are compared with the theory at constant velocities, $v = 0.41v_0$, $0.63v_0$, and $0.91v_0$. In some cases, it was necessary to extrapolate the measured curve in order to find the S_e values at all three velocities. The extrapolations were carried out on the assumption that $S_e = kE^p$. As may be seen from Fig. 6, the earlier reported oscillations ($Z_1 \leq 20$) of S_e are also present in the extended Z_1 range. The amplitudes of the oscillations increase slightly with Z_1 . This was unexpected, since the statistical Thomas-Fermi treatment predicting a smooth S_e curve should be more appropriate at higher Z_1 values. The theoretical curve by Lindhard and Scharff,³ however, represents a good mean value to the experimental data for all Z_1 . The oscillations of S_e are presumably correlated to the ionic shell structure of the penetrating ions. The data, however, do not reveal a simple correlation. For example, Ne is positioned on the mean value of the S_e curves and Na just below, whereas Ar and K are close to the maximum. Kr, again, is positioned on the mean value. From Fig. 6, it is also apparent that the wavelength

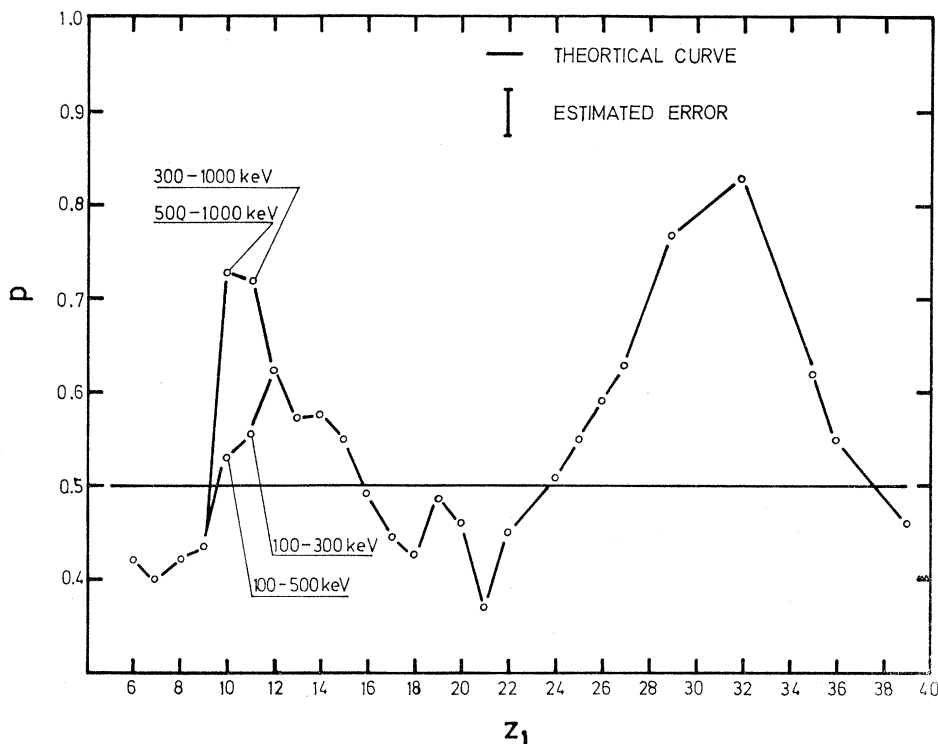


FIG. 5. Exponent p in $S_e = kE^p$ against Z_1 .

in Z_1 units of the oscillations increases with increasing Z_1 . The relative size of the amplitudes decreases with increasing common velocity. Deeper interpenetration of atomic shells at higher velocities presumably causes the shell effect to become less important.

Range studies by Eriksson *et al.*¹¹ in an oriented tungsten monocrystal show oscillations similar to those observed for amorphous targets. Their results for $11 \leq Z_1 \leq 37$, converted to stopping cross sections at $v = 0.63$, are also displayed in Fig. 6. The channeling

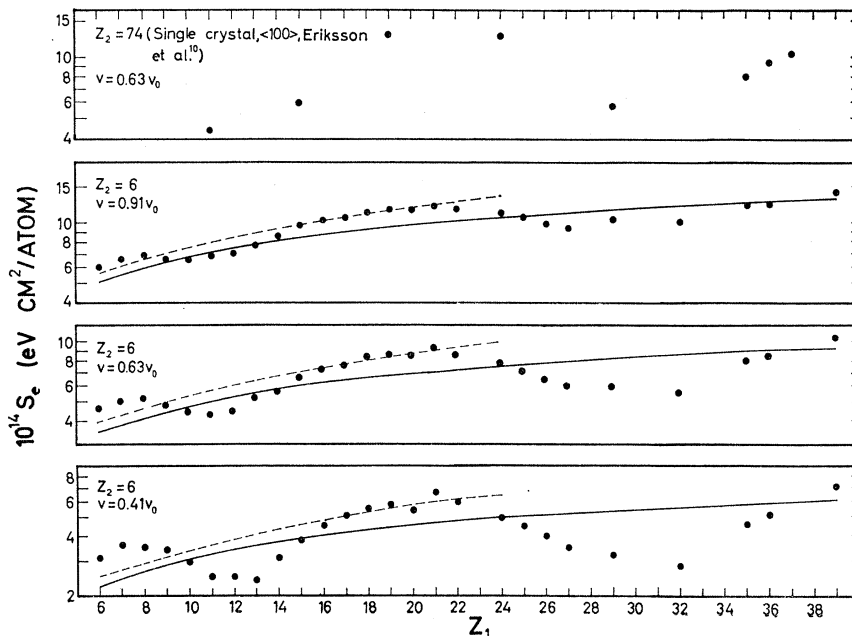


FIG. 6. Electronic stopping cross section S_e versus Z_1 for three constant common velocities. The data for $v = 0.41 v_0$ and $Z_1 < 18$ are taken from Ormrod *et al.* (Refs. 6 and 7). Solid and dashed curves indicate theoretical curves by Lindhard and Scharff (Ref. 3) and by Firsov (Ref. 4), respectively.

TABLE II. The relative amplitudes (%) of the S_e oscillations around the Lindhard-Scharff curve^a. The data for $Z_2=5$ and 13 are taken from Ormrod *et al.*^b and the data for $Z_2=73$ are taken from Eriksson *et al.*^c

	Amplitudes at Z_1			
	1st max.	1st min.	2nd max.	2nd min.
$V=0.41 V_0$				
$Z_2=5$ (amorphous)	50% ($Z_1\sim 7$)			
$Z_2=6$ (amorphous)	46% ($Z_1\sim 7$)	36% ($Z_1\sim 12$)	55% ($Z_1\sim 21$)	51% ($Z_1\sim 32$)
$Z_2=13$ (amorphous)	25% ($Z_1\sim 7$)			
$V=0.63 V_0$				
$Z_2=6$ (amorphous)	32% ($Z_1\sim 7$)	17% ($Z_1\sim 12$)	$\sim 40\%$ ($Z_1\sim 21$)	33% ($Z_1\sim 32$)
$Z_2=73$ (aligned $\langle 100 \rangle$ crystal)		$\sim 50\%$ ($Z_1\sim 12$)	$\sim 50\%$ ($Z_1\sim 21$)	$\sim 50\%$ ($Z_1\sim 32$)
$V=0.91 V_0$				
$Z_2=6$ (amorphous)	22% ($Z_1\sim 7$)	9% ($Z_1\sim 12$)	28% ($Z_1\sim 21$)	17% ($Z_1\sim 32$)

^a The amplitudes in the tungsten case (aligned $\langle 100 \rangle$ crystal) are taken relative to the mean value of the experimental data.

^b References 6 and 7.

^c Reference 11.

of the ions results in an almost complete absence of the nuclear stopping and, in comparison with the amorphous tungsten case, it causes a reduction to approximately one third of the electronic stopping cross section.

Table II summarizes our previous and new results together with the results of Ormrod *et al.*^{7,8} in amorphous targets and those of Eriksson *et al.*¹¹ in an oriented tungsten crystal.

A few observations can be made:

(1) The relative amplitude of S_e for the maximum at $Z_1=7$ tends to decrease with increasing Z_2 for amorphous targets.

(2) In the tungsten crystal, the S_e oscillations for the channeled beam have anomalously large amplitudes compared with amorphous targets.

(3) The positions of the maxima and minima of the S_e oscillations for amorphous targets with $Z_2=5, 6,$ and 13 are the same as the positions for the crystalline tungsten target with $Z_2=73$.

(4) The relative amplitudes of S_e decrease with increasing common velocity.

We conclude that the positions of the maxima and minima of S_e are insensitive both to Z_2 and to the beam being either channeled or random. The relative ampli-

tudes of the S_e oscillations appear to be correlated to the degree of interpenetration of atomic shells during the collisions, i.e., the relative amplitudes decrease with increasing ion velocity and increase if the ions are channeled. We do not have a simple explanation of the fact that the relative amplitudes of the S_e oscillations increase with Z_1 , but we suggest that a possible nonmonotonic change in the capture and loss cross sections of the ions against Z_1 may be at least partly responsible for the effect.

The influence of the charge state of the incoming or emerging ions on the observed stopping cross section was studied in some detail. In no cases was the effect greater than a few per cent, which is consistent with the observations made in I.

ACKNOWLEDGMENTS

Grateful thanks are extended to K. O. Nielsen for his continuous support and to the members of the technical staff of the heavy-ion accelerator for their great help in this work. Numerous discussions with J. A. Davies at the initial stage of this work are also gratefully acknowledged. This work was financially supported by the Danish State Research Foundation.